International Journal of Geographical Information System Applications and Remote Sensing

"المجلة الدولية لتطبيقات نظام المعلومات الجغرافي والاستشعار عن بعد"

Vol. 1, No. 1, July2010
ISSN **2077-771X***; Copyright © ICSRS Publication, 2010*
www.i-csrs.org

Multi-sensors, Multi-resolution Data Fusion Using Principal Components Analysis and Histogram Specification Techniques

Saleh Mahdi Ali

Remote Sensing Research Unit, College of Science, University of Baghdad, Iraq, Baghdad, Al-Jaderyia
e-mail: Sensing.remote@gmail.com

Abstract

Image data fusion is the process of setting together information gathered by different heterogeneous sensors, mounted on different platforms. This paper presents an effective multi-resolution image data fusion methodology, which is based on utilizing the Principal Component Analysis "PCA" and Histogram Specification "HS" techniques. The first principal component "PCA1" involves much of the variability in the spectral data; while the reminder PCAs contain the remaining variability in a descend order. In this research, the low resolution multispectral are, firstly, resized (i.e. enlarged) into the high resolution "panchromatic" image size, then transformed into several PCAs. The high resolution panchromatic image should be normalized to have the same number of gray levels as the PCA1. The renormalized panchromatic image, then, replace the PCA1 of the low- resolution-multispectral image in the PCA transformed domain. The preliminary high-resolution-multispectral images are produced by inversely transform the modified PCA's file. The final high-resolution-multispectral bands are created by pushing the histogram of each created image bands toward the histogram of its corresponding original multispectral band, utilizing the histogram-specification method.

Keywords: image fusion, PCA transformation, histogram specification.

1 Introduction

In recent years, many solutions for multi-resolution image data fusion have been proposed, for instance see [1-6]. In remote sensing applications, the increasing availability of space borne sensors gives a motivation for different image fusion algorithms. Several situations in remote sensing require high spatial and high spectral resolutions being existed in a single image. Most of the available equipments are not capable to provide such data. Therefore, image fusions may be used to provide the integration of different information sources; i.e. the fused image can have complementary spatial and spectral resolution characteristics. Generally, the standard image fusion techniques distort the spectral information of the multispectral data; mostly they fall into two categories; i.e. ***feature space*** and ***spatial domain*** techniques [7]. The feature space fusion is performed by transforming the multispectral images into a new space in which one image represents the correlated component; e.g. the PCA1, using the PCA transformation, or adopting the intensity in a space created with Color-Space Transform (CST). In both these methods, the correlated component is replaced by the higher resolution image and transforms the result back to the image space. However, the spatial domain fusion techniques transfer the high-frequency contents of the higher-resolution image to the lower resolution image. In best cases, the mentioned methods have not satisfied enlargement more than 7.5:1 times, see the table at chapter-8, pp.373-374 of Schowengerdt[7].

Normally, the problem of image data fusion comes when different sensors imaging the same object and we try to obtain a result that integrates the best characteristics of each of those sensors. In this research, to overcome this problem, our fusion technique will concern on improving both the spatial characteristic (utilizing PCA), and enhancing the spectral characteristic (using the HS).

2 The PCA Transformation

The PCA is a feature space transformation method designed to remove the redundancies existed between similar functions or images. It is a linear transform of the type[8].

$$PCA = W_{PCA} . Y \tag{1}$$

Where; *PCA* is the output principal component vector, *Y* is the image spectral vector, and W_{PCA} is a weight matrix, referred as the transformation kernel, represented as;

$$W_{PCA} = \begin{bmatrix} e_1^T \\ . \\ . \\ e_K^T \end{bmatrix} = \begin{bmatrix} e_{11} & . & . & e_{1K} \\ . & & & . \\ . & & & . \\ e_{K1} & . & . & e_{KK} \end{bmatrix} \quad (2)$$

Where: e_{ij} is the j^{th} element of the i^{th} covariance matrix eigenvector.

This transformation kernel alters the covariance matrix *C* as follows;

$$C_{PCA} = W_{PCA} C W_{PCA}^T = \begin{bmatrix} \lambda_1 & . & . & . & 0 \\ . & \lambda_{21} & . & . & . \\ . & . & \lambda_3 & . & . \\ . & . & . & . & . \\ 0 & . & . & . & \lambda_K \end{bmatrix} \quad (3)$$

The zero values of the off-diagonal elements refer to that; the elements of the *PCA* vectors are uncorrelated. Keep in mind that λ_K are the eigenvalues of *C* can be found as the roots of the following characteristic equation[7];

$$| C - \lambda I | = 0 \quad (4)$$

Where: *I* is the diagonal identity matrix.

The *PCA* coordinate axes are defined by the *K* eigenvectors e_K, that can be obtained from the following vector-matrix equation, for each eigenvalue $\lambda_{i;}$ i.e.

$$| C - \lambda_i I | e_i = 0; \quad for \ i = 1,2,...,K \quad (5)$$

3 Histogram Specification Technique

Particularly, it is useful sometimes to be able to specify the shape of the histogram that we wish to process an image to have it; the method is called ***histogram matching*** or ***histogram specification[9]***. Let we have consider continuous gray levels r and a continuous random variables z, and let $p_r(r)$ and $p_z(z)$ denote their probability density functions. In this notation, r and z denote the gray levels of the input and output (processed) images, respectively. We can estimate $p_r(r)$ from the given input image, while $p_z(z)$ is the specified probability density function "pdf" that we wish the output image to have. Let *s* be a random variable with the property;

$$s = T(r) = \int_0^r p_r(w)\,dw \tag{6}$$

Where *w* is a dummy variable of integration.

Similarly, suppose we define another random variable *z* with the property;

$$G(z) = \int_0^z p_z(t)\,dt = s \tag{7}$$

It then follows from the above two equations that; *z* must satisfy the following condition;

$$z = G^{-1}(s) = G^{-1}[T(r)] \tag{8}$$

The discrete formulations of the above equations are as follows[9]:

For equation(6);

$$s_k = T(r_k) = \sum_{j=0}^{k} p_r(r_j) = \sum_{j=0}^{k} \frac{n_j}{n} \quad , \quad k = 0,1,2,..., L-1 \tag{9}$$

For equation(7);

$$G(z_k) = \sum_{j=0}^{k} p_z(z_j) = s_k \quad , \quad k = 0,1,2,..., L-1 \tag{10}$$

Finally the discrete version of equation(8) is;

$$z_k = G^{-1}(s_k) = G^{-1}[T(r_k)] \quad , \quad k = 0,1,2,....., L-1 \tag{11}$$

Where *n* is the total number of pixels in the image, n_j is the number of pixels with gray level r_j, and *L* is the number of discrete gray levels.

4 Samples of the used Images

The used samples of images represent the Campus of Baghdad University with different spatial resolutions. The low-resolution-multispectral bands, acquired by Landsat-7 satellite imagery with the Enhanced Thematic Mapper "ETM_+" sensor (Dated 2000, Spatial Resolution 14.25m), and their "RGB" colored version (Blue 0.45-0.52 µm, Green 0.52-0.6 µm, and Red 0.63-0.69 µm) are shown in fig.1. Figure.2 represents their histograms. The high-resolution image, representing the same area, acquired by QuickBird satellite imagery, pan-sharpened (0.6m, dated 2003), and its histogram are shown fig.3. The studied area lies between the

latitudes 33.2987°N to 33.257°N and longitudes 44.356°E to 44.415°E, using UTM projection, WGS84 Datum (Zone 38 Northern Hemisphere), and covering an area of approximately 25.685 km^2.

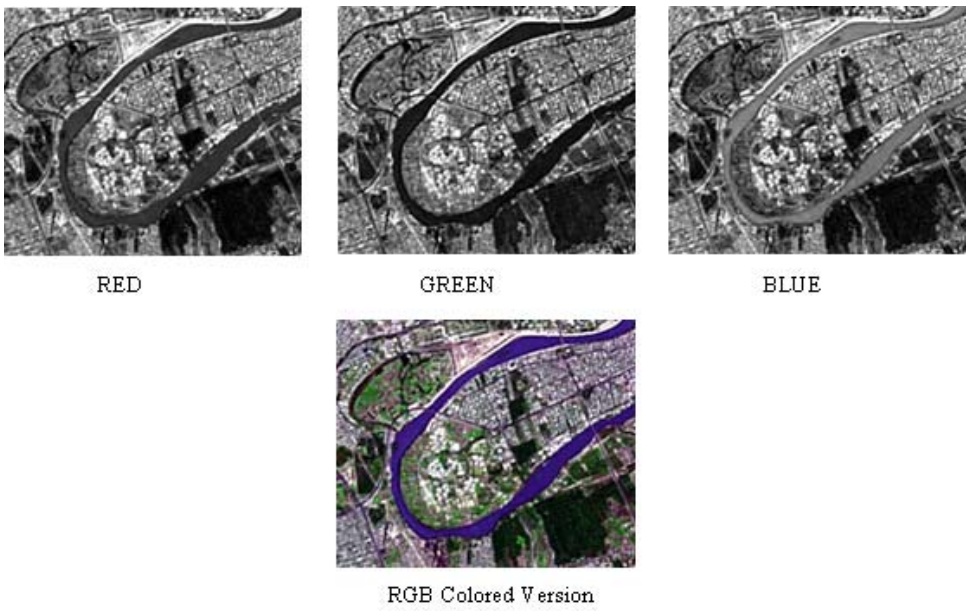

Figure-1: The ETM$_+$ RGB bands, their colored combination, each of size 388×326 pixels.

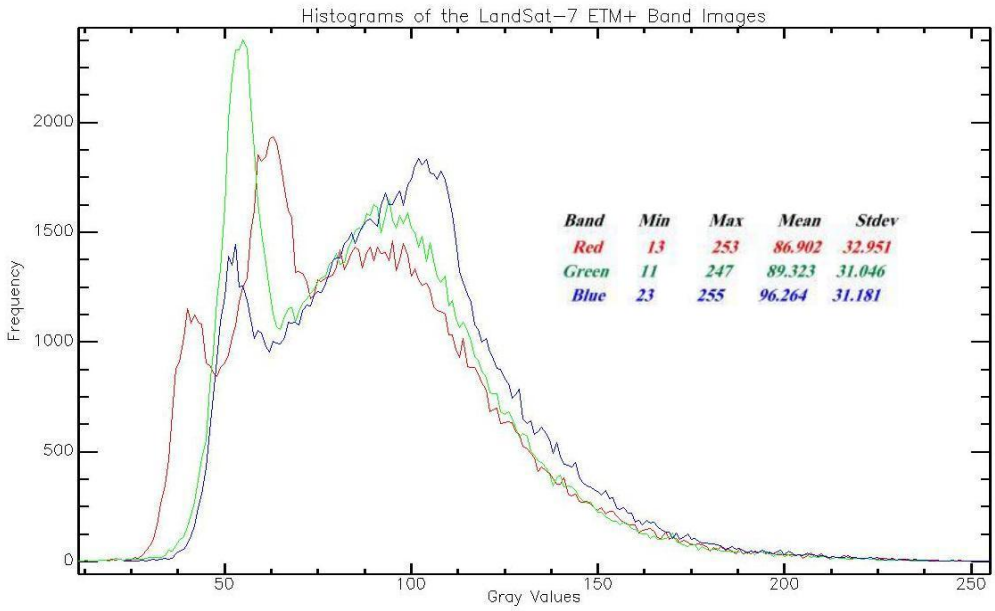

Figure.2: Histograms of the Low-Resolution-Multispectral (ETM$_+$), RGB bands.

a) QuickBird (0.6m, size 9217x7745 pixels) image

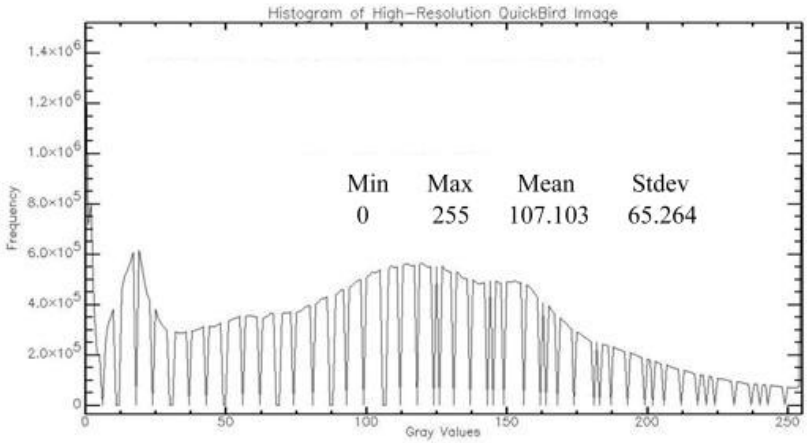

b) Histogram of the QuickBird Image

Figure.3: The QuickBird panchromatic (0.6m) image and its histogram.

5 Experimental Results

As it has been mentioned in the abstract, the first step is to resize the low-resolution-multispectral bands (388×326 pixels) to have the same size as the high-resolution panchromatic (9217×7745 pixels) image. Here, the ***bilinear methodology[10]*** is used to enlarge the smaller size ETM_+ bands to the larger QuickBird size (about 23.758 times). Figure.4 shows the enlarged colored bands and their histograms.

a) The enlarged color bands of ETM+

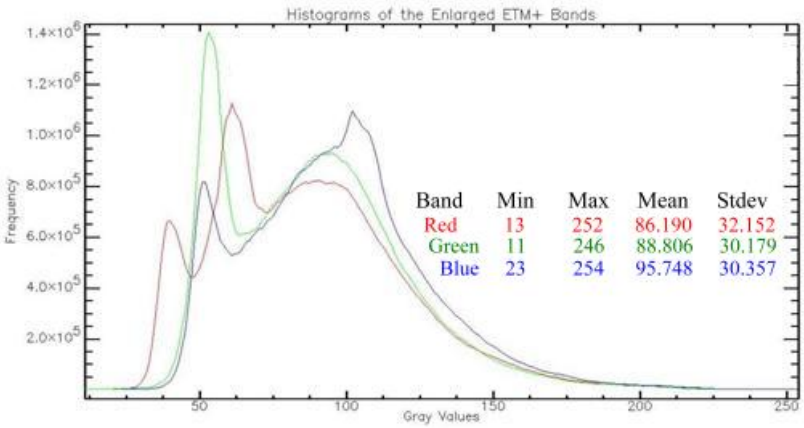

b) Histograms of the Enlarged ETM+ bands Image

Figure.4: The enlarged bands of the ETM_+ and their histograms.

The principal components of the resized bands have been computed and illustrated with their histograms in figs.5, 6 and 7, respectively. The statistical characteristics of the three PCAs are listed in Table-1. To produce the high-resolution-multispectral bands, the first principal components "***PCA1***" shown in fig.5 should be replaced by the renormalized version of the QuickBird image shown in fig.2.

a) The PCA1 image of the enlarged ETM+ bands

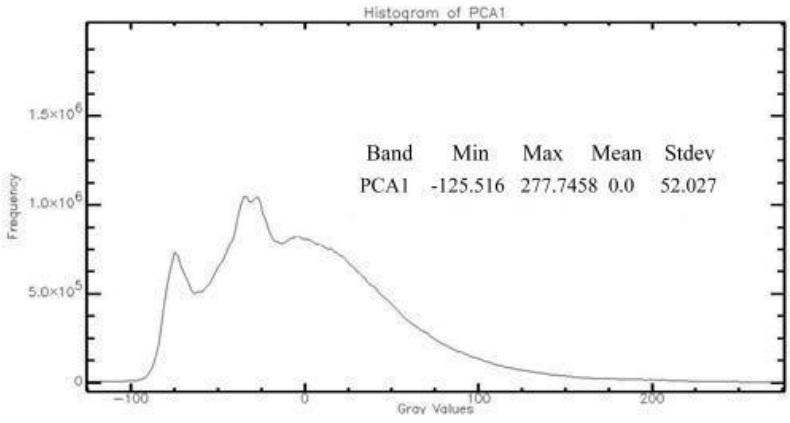

b) The PCA1 histogram of the enlarged ETM+ bands

Figure.5: The PCA1 image of the enlarged ETM_+ bands and its histogram.

a) PCA2 of the enlarged ETM+ bands

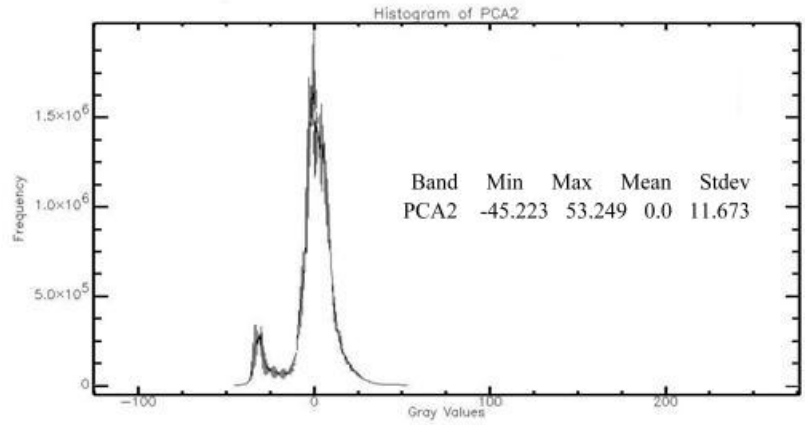

b) The PCA2 histogram of the enlarged ETM+ bands

Figure.6: The PCA2 image of the enlarged ETM_+ bands and its histogram

a) The PCA3 image of the enlarged ETM+ bands

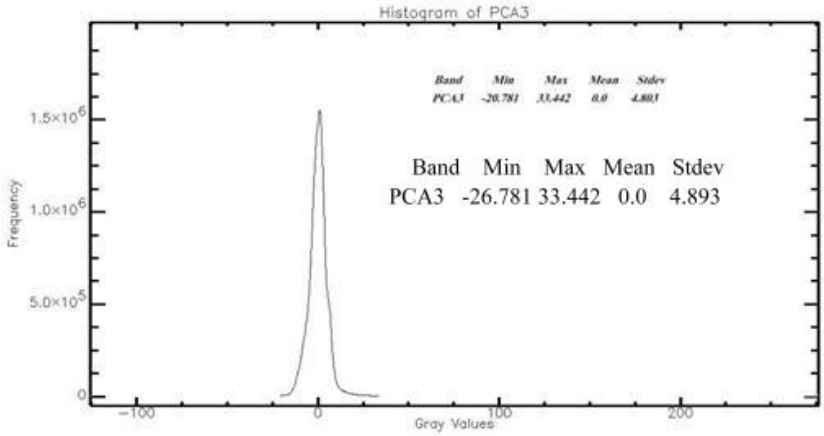

b) The PCA3 histogram of the enlarged ETM+ bands

Figure.7: The PCA3 image of the enlarged ETM_+ bands and its histogram

Let $f_{in}(x, y)$ and $f_{out}(x, y)$ represent, respectively, the original and the normalized QuickBird image gray values, using.

$$f_{Out}(x,y) = \frac{f_{in}(x,y) - Min_{QuickBird}}{Max_{QuickBird} - Min_{QuickBird}} \times (Max_{PCA1} - Min_{PCA1}) + Min_{PCA1} \qquad (12)$$

The normalized version of the QuickBird image ant its histogram is shown in Fig.8.

a) The normalized version of the QuickBird image.

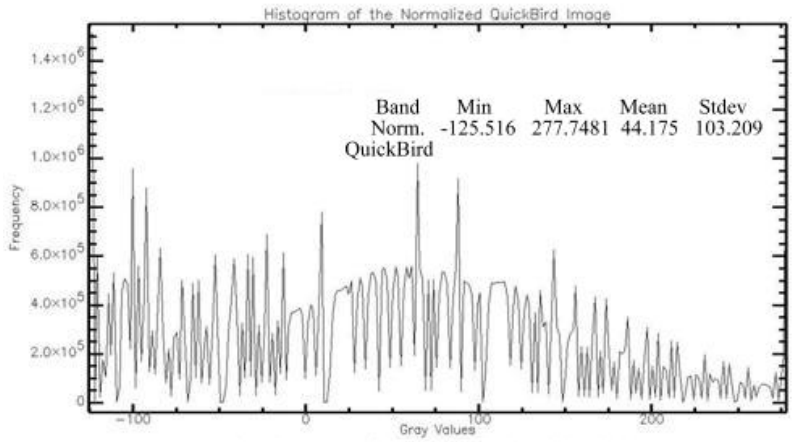

b) Histogram of the normalized QuickBird image.

Figure.8: The normalized version of QuickBird image and its histogram.

The preliminary production of the high resolution multispectral QuickBird bands can now be produced by replacing the PCA1 image (shown in fig.5a) by the normalized QuickBird image (shown in fig.8a), and performing PCA's inverse transformation. The resulted QuickBird multispectral bands obtained from the PCA inverse transformation and their histograms are illustrated in fig.9.

a) The RGB bands of the preliminary produced QuickBird

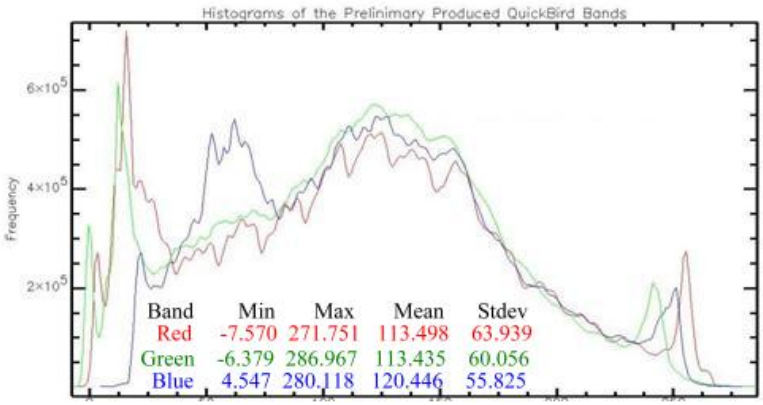

b) Histogram of the RGB bands of preliminary QuickBird

Figure.9: The preliminary produced version of the high resolution QuickBird bands image and their histograms.

The final step in our present research is to push the gray distribution values of the reproduced high-resolution bands (shown in fig.9b) toward the distribution of the enlarged bands of the original ETM_+ images (shown in fig.4b). Before proceeding further in this step, let us inspect carefully the statistical features of the image bands to be matched, as illustrated in fig.10. The first in our matching process is to normalizing the reproduced high-resolution bands to have the same gray distribution ranges as of the enlarged bands, using:

$$f_{Nor}(x,y,i) = Round\left(\frac{f_{QB}(x,y,i) - Min_{QB}}{Max_{QB} - Min_{QB}} \times (Max_{En} - Min_{En})\right) + Min_{En} \qquad (13)$$

Where: $f_{Nor}(x,y,i)$ represents the output normalized i^{th} band, $f_{QB}(x,y,i)$ is input reproduced QuickBird band, Max_{QB}, Min_{QB}, Max_{En}, and Min_{En} are, respectively, the maximum and minimum values of the QuickBird and the Enlarged bands.

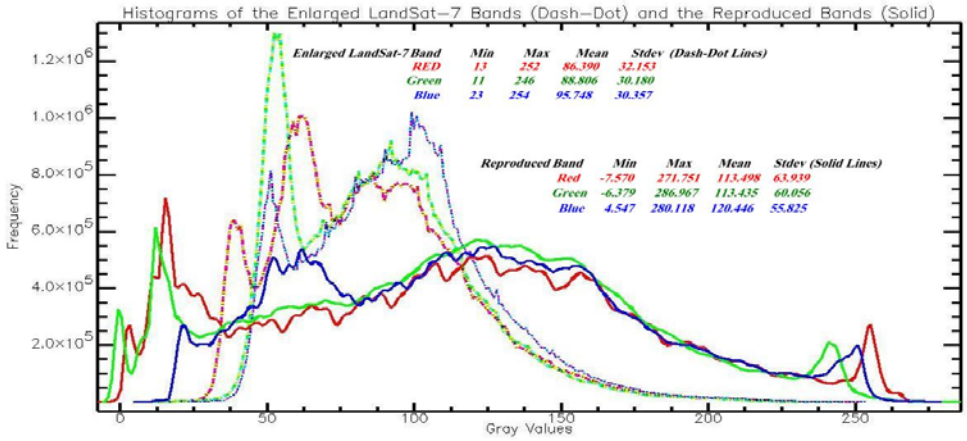

Figure.10: illustrates the gray distributions of the images to be matched.

Figure.11, illustrates the input and output gray distribution values obtained from Eq.(13), while Table-2 list the statistical features of these gray distributions. The final step is performed by utilizing Eq.(11) and pushing the normalized QuickBird distribution bands toward the enlarged distribution bands. The final produced high-resolution QuickBird bands are illustrated with their histograms, respectively, in figs.12a &b. For the purpose of comparison, the statistical features of the final produced high-resolution QuickBird bands are listed in Table-3. It is easy to deduce the similarities between the final produced and the original enlarged bands (shown in Tables-2&3).

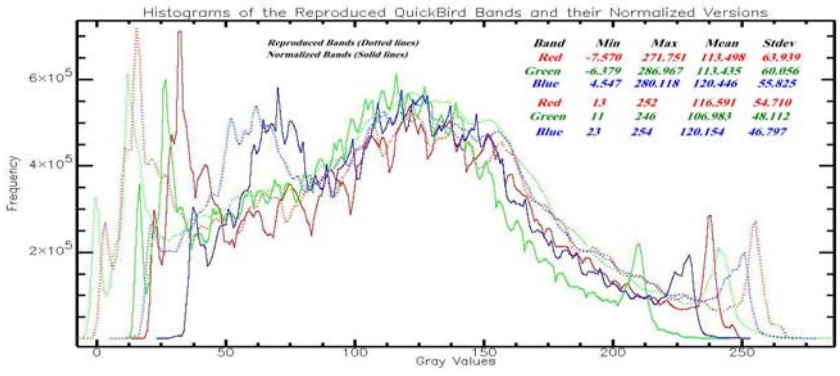

Figure.11: illustrates the gray distributions of the original reproduced QuickBird bands and their normalized versions.

a) The final produced RGB QuickBird bands

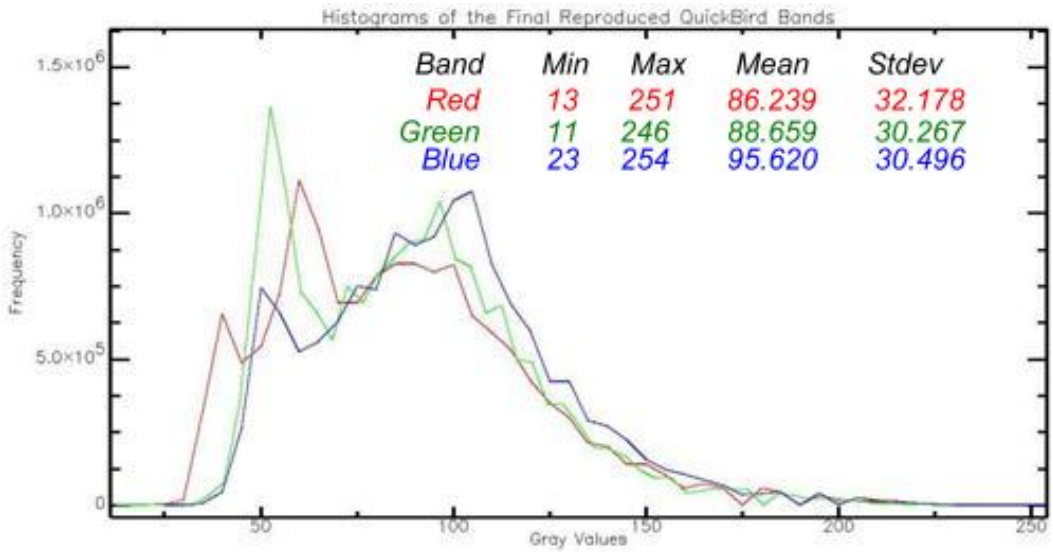

b)Histograms of the final produced RGB QuickBird bands

Figure.12: The final produced version of the high resolution QuickBird bands; a) image, and b) their histograms.

Table 1: The statistical characteristic of the PCA's of the enlarged ETM+ bands.

PCA	Min	Max	Mean	Stdev	Eigenvalues λ_i	Energy $\lambda_i/\lambda_{total}$
1	-125.515633	277.745819	0.0	52.027227	2706.832297	94.44 %
2	-45.223461	53.248730	0.0	11.673224	136.264160	4.75%
3	-20.780693	33.441925	0.0	4.802744	23.066348	0.81%
Total					2866.162805	100%
Note: last column represent the amount of image information that can be obtained by adopting each of the PCA in an inverse PCA's transformation process.						

Table 2: The statistical features of the gray distribution of the image bands shown in figs.10&11.

Image name	Band name	Bin-size	Bin numbers	Min value	Max value	Mean value	Stdev value
Enlarged Bands of ETM+ Images	Red	1	240	13	252	86.389947	32.153117
	Green	1	236	11	246	88.806048	30.179703
	Blue	1	232	23	254	95.748008	30.356636
Reproduced High-Res. QuickBird Bands	Red	1.0997	255	-7.56972	271.751007	113.497848	63.939181
	Green	1.1549	255	-6.37874	286.966827	113.434840	60.056494
	Blue	1.0849	255	4.547344	280.117828	120.446427	55.825041
The Normalized QuickBird Bans	Red	1	240	13	252	116.591094	54.710140
	Green	1	236	11	246	106.983061	48.112371
	Blue	1	232	23	254	120.153556	46.796850

Table 3: The statistical features of the gray distributions for the final high-resolution QuickBird bands shown in fig.12.

Image name	Band name	Bin-size	Bin numbers	Min value	Max value	Mean value	Stdev value
Final Produced Bands of the High-Res. QuickBird Bands	Red	1	239	13	251	86.238791	32.377901
	Green	1	236	11	246	88.658726	30.366838
	Blue	1	232	23	254	95.620146	30.496099

6 Conclusions

High resolution multispectral bands are very valuable for too many applications in remote sensing; they can efficiently use to predict the crop production, monitoring vegetation health condition, for desertification researches, production of high-resolution topographic and photometric maps etc. Unfortunately, high-resolution-multispectral-sensors are not available. Therefore, multispectral bands with high-resolution possessions are too costly. For these reasons our presented research insisted to produce multispectral bands having concurrent behaviors as the original lower-resolution bands. The simulation procedure in this research is based on three very important concepts; the first was the enlargement operation which is performed by the bilinear interpolation method and not other lower or higher order interpolation techniques. The suitability of this adoption can be clarified by comparing the image band histograms illustrated in figs.2 & 4b. The second adopted process was the implementation of the PCA transformation which is, normally, produced PCA1 band consisting, almost, the whole correlated information involved in the transformed bands. Thus, replacing the PCA1 by the gray's normalized high-resolution image insured the produced inversely transform bands to consist most of the important information existed in the original low-resolution multispectral bands, for instance see figs.5a & 8a. Finally, the histogram specification technique matched, well, the band's features, as illustrated in figs.4b & 12b. It is remain to be mentioned that; we used the enlarged bands in the histogram matching process (i.e. not the original multispectral bands), because they have the sizes, and thus easier for comparison purposes.

References

[1] J. Zhou, , D.L. Civco and J.A. Silander, "A wavelet transforms method to merge Landsat TM and SPOT panchromatic data," International Journal of Remote Sensing 19(4):743-757 (1998)

[2] B. Zhukov, D. Oertel, F. Lanzl and G. Reinhackel," Unmixing-based multi-sensor multi-resolution image fusion," IEEE Transactions on Geosciences and Remote Sensing 37(3): 1212-1226 (1999).

[3] J.G. Liu,, "Smoothing filter-based intensity modulation: A spectral preserve image fusion technique for improving spatial details," International Journal of Remote Sensing 21(18): 3461-3472 (2000).

[4] M., Lillo-Saavedra, C. Gonzalo, A. Arquero, and E. Martinez, "Fusion of multispectral and panchromatic satellite sensor imagery based on tailored filtering in the Fourier domain," International Journal of Remote Sensing 26(6): 1263-1268 (2005).

[5] T. Bretschneider, and O. Kao, "Image fusion in remote sensing," Proceeding of the 1st online, symposium of computer engineering (2000).

[6] B. Vladimir, “Image and information fusion in remote sensing,” 1st year (progress report, school of computer engineering, 2004)
[7] A. R. Schowengerdt, “Remote Sensing: Models and Methods for Image Processing,” 3rd ed. (Academic Press, 2007).
[8] B. Noble, and J. W. Daniel, “Applied Linear Algebra,” 3rd ed. (Prentice Hall, Upper Saddle River, 1988).
[9] R.C. Gonzalez, and R.E. Woods, “Digital Image Processing,” 2nd ed. (Prentice Hall, Upper Saddle River, New Jersey 07458, 2002)
[10] T. M. Lillesand, and R. W. Kiefer, “Remote Sensing and Image Interpretation,” 3rd ed. (John Wiley and Sons,